Measured Responses of a Corrugated Steel Ellipse Culvert at Different Cover Depths

Oliver Kearns[1]; Ian D. Moore, M.ASCE[2] Neil A. Hoult, M.ASCE[3];

Abstract: Typical design and installation methods for corrugated steel culverts involve consideration of a minimum burial depth and most current North American design codes consider failure only due to excessive circumferential force in the conduit walls (i.e. hoop thrust). However, recent studies have shown that bending moment is often the more dominant behaviour for corrugated steel culverts at shallow cover. To address this issue, an elliptical corrugated steel culvert was tested under simulated vehicle loading at depths ranging from 0.1 m to 1.2 m. The results show that, under a wheel pair load, a peak negative bending moment and thrust force are consistently developed at the crown with positive bending moments adjacent to the crown and near the shoulders. When the flexural and circumferential force results are extrapolated to the yield point and compared, the bending moment values are up to 5 times larger than the yield limit while thrust values are only 60% of the limit. The test results suggest that bending moments should be considered during the design and installation of corrugated steel culverts at shallow cover.

Keywords: culverts, shallow cover, full-scale experiment, live loading, distributed strain

[1] Researcher, GeoEngineering Centre at Queen's-RMC, Queen's University, Kingston, ON, Canada K7L 3N6. E-mail: oliver.kearns@queensu.ca
[2] Professor and Canada Research Chair in Infrastructure Engineering, GeoEngineering Centre at Queen's-RMC, Queen's University, Kingston, ON, Canada K7L 3N6. E-mail: ian.moore@queensu.ca
[3] Associate Professor, Dept. of Civil Engineering, Ellis Hall, Queen's University, Kingston, ON, Canada K7L 3N6. E-mail: neil.hoult@queensu.ca (corresponding author)

Introduction

For many years corrugated steel culverts with conventional corrugation geometries (having wavelengths or pitches of 152 mm or less) have been designed with a focus on buckling and wall crushing caused by circumferential force as the main failure mechanism. Flexural responses, such as local bending and plastic hinge formation, have been deemed less critical and have received little to no attention in the existing Canadian (CSA 2017a) and American (AASHTO 2017a) design standards. However, recent experimental measurements have shown how bending moment contributes to the overall response more than generally recognized, and that plastic hinge mechanisms can control the capacity of these structures at shallow cover where wheel loads at the ground surface induce local bending in the culvert (Regier et al. 2017). Previous researchers have suggested that burial depth and bending moment play a critical role in the capacity of metal culverts. Duncan (1978) was one of the first to establish various minimum burial and maximum fill recommendations for metal culverts with different geometries based on finite element models and published construction measurements. As non-linear finite element software packages improved, finite element analyses examining the stability of shallow buried culverts subjected to excessive vehicle loads became more common (Seed and Raines 1988). However, several studies observed that a load applied to the surface directly above a metal culvert creates a complex three dimensional response that cannot be accurately captured by more simplistic two dimensional models (Moore and Brachman 1994; Taleb and Moore 1999; El-Sawy 2003), emphasizing the need for further research at shallow cover depths. More recently, Yeau et al. (2009) performed an extensive field testing program involving 39 in service long span (greater than 3 m) metal culverts under static and dynamic live loading to assess the structural capacity and deformation. That project quantified how deflections vary nonlinearly with burial depth and demonstrated that the most extreme deflection and strain behaviours occurred at depths less than 2.5 m (shallow cover).

Meanwhile, field research by Sezen et al. (2008) on long span metal culverts and experimental research projects by Mai et al. (2014) and Regier et al. (2018) on short span metal culverts have shown that bending moments near the crown often create the dominant stress resultant, not thrust, especially at shallow cover depths. In fact, tests performed by Regier et al. (2017) and Tetreault et al. (2018) have found that a short span elliptical culvert loaded to its ultimate limit state can fail in flexure due to plastic hinge formation around the top of the culvert instead of buckling or wall crushing caused by thrust. To date, shallow burial tests have been conducted at one or two cover depths and often involve other variables such as wall deterioration (Regier et al. 2017; Tetreault et al. 2018), while field research requires testing multiple different culverts to gather information regarding variables such as cover depth and often neglects any bending moments, opting to focus solely on thrust behaviour (Sargand et al. 2018; Yeau et al. 2009; Yeau and Sezen 2012).

According to the Canadian Highway Bridge Design Code [CHBDC (CSA 2017b)] and the American Association of State Highway and Transportation Officials (AASHTO 2017a), culverts require a minimum burial depth to protect against premature failure caused by surface loading. However, there is still a lack of understanding about the behaviour of corrugated steel culverts as cover depths increase and ultimately transition to 'deep burial' responses. Additionally, the current design method in the Canadian code does not apply to metal culverts with spans less than 3 m, (implicitly defined as short span structures) (CSA 2017a), despite the frequent use of these structures as bridges. To the authors' knowledge, there have been no experiments conducted on an intact metal culvert with a span less than 3 m and under multiple shallow burial depths, that have investigated both thrust and flexure. This presents the possibility that, for projects where shallow cover exists, there is the potential for the culvert to have an unconservative design focussed on the wrong stability limit state and leading to the potential for premature failure due to bending. Load ratings for existing culverts will also be deficient if they examine hypothetical limit states that do not control stability, and improvements in the understanding of the mechanisms that control capacity are likely to improve the efficiency and safety of load ratings.

The objectives of this research project are to (1) investigate the change in behaviour as the burial depth transitions from shallow cover to deep cover, (2) investigate the impact of increasing static live loading on culverts with variable cover depths, (3) examine whether the vertical diameter change induced by combined earth and surface load meets the serviceability limit state at each depth, and (4) assess the implications and appropriateness of the current minimum cover depths used for national highways in Canada and the US. This paper describes the tests conducted on a corrugated steel culvert with a horizontal ovality and investigates the behaviour under simulated vehicle loading. The next section of the paper discusses the experimental method, including the test set up, culvert specimen, burial method and surface loading procedure. The results of the investigation will then be presented and discussed highlighting all key conclusions.

Experimental Methods

Test Overview

A horizontal ellipse culvert was buried in well compacted granular soil in the 8 m long, 8 m wide and 3 m deep test pit described by Moore (2012). This specimen was tested with cover depths ranging from 0.1 to 1.2 m increasing in steps of 0.2 m up to 0.9 m with a final increase of 0.3 m, for a total of 6 tests. Static service load was applied using a 2000 kN hydraulic actuator acting on a steel plate at the ground surface and was applied in 3 cycles. Each cycle began at 0 kN, the load was then increased to the predetermined load limit, and then decreased to 0 kN. These loading cycles were used at each depth to record the initial inelastic response during cycle 1 and the elastic reloading and unloading responses during cycles 2 and 3.

Test Configuration

The culvert was placed on a loose bedding material in the East-West orientation (Figure 1a) with distances of 3.20 m, 3.20 m, and 1.55 m between the culvert edge and the South, North, and West pit walls, respectively (Figure 1b). Concrete blocks were used at the West end of the pit to confine the soil and allow access to the end of the culvert. The hydraulic actuator was positioned under a stiff reaction frame above the crown of the culvert at a distance of 4 m from the West end of the test pit. The load from the actuator was applied to a 0.6 m by 0.25 m steel plate on the soil surface which simulates a single wheel pair directly above the crown (as defined in CSA 2017a). Figure 1(c) shows an elevation view of the test configuration and the test pipe.

Culvert Specimen

The culvert specimen had a length of 6450 mm and an initial 8% horizontal ovality, and was loaded vertically before burial to induce an 11% ovality with span of 1650 mm and rise of 1300 mm (Figure 1c). It was manufactured using shallow bolted corrugated steel plates with an amplitude of 25 mm, a wavelength of 75 mm, a design wall thickness of 1.82 mm, and an assumed modulus of elasticity of 200 GPa. The cross-sectional properties per unit length were an area, A, of 2.259 mm^2/mm, second moment of area, I, of 170.4 mm^4/mm, and section modulus, S, of 12.52 mm^3/mm according to the Corrugated Steel Pipe Institute Handbook (2010). In addition, the yield strength of the steel was taken to be 230 MPa as per ASTM A929 (2018). The Canadian code classifies minimum burial for a corrugated metal culvert based on the amplitude of the corrugations and the vertical and horizontal diameters of the structure (CSA 2017b) as given in Equation (1).

$$H_{min} = max\begin{cases} 0.6 \\ \frac{D_h}{6}\left[\frac{D_h}{D_v}\right]^{0.5} \\ 0.4\left[\frac{D_h}{D_v}\right]^2 \end{cases} \tag{1}$$

While the American code classifies minimum cover based on the span alone as per Equation (2) [from Table 12.6.6.3-1 in AASHTO (2017a)],

$$H_{min} = \frac{S}{8} \geq 12.0\ in\ (0.3\ m) \tag{2}$$

where H_{min} is the distance, in metres, from the road surface to the crest of the corrugation at the crown, D_h is the horizontal diameter, D_v is the vertical diameter, and S is the span (horizontal diameter). Normally, the Canadian minimum burial depth equation only applies to culverts with span greater than 3 m, however for the purpose of this study the equation was assumed applicable to all culvert sizes. This meant the minimum permitted cover for this structure would be 0.6 m or 0.3 m based on the Canadian and American codes, respectively.

Backfill Procedure

All backfill material for the experiment consisted of a poorly graded sandy gravel (GP-SP) as classified by ASTM D2487-17 (2017). First a 300 mm thick compacted base was established within the pit followed by a 75 mm loose base to prevent the invert from lifting off the base during compaction. Then backfill was placed around the culvert in 200 mm compacted lifts until the first burial depth (0.1 m above the crown) was achieved. Each lift was compacted in a spiral path starting at the outer edges using a vibrating plate tamper (Wacker wp1550AW, Wacker Corp., Menomonee Falls, Wisconsin), aiming for 90% standard Proctor compaction as monitored by a model MC1DR-P nuclear densometer (CPN International, Inc., Concord, California). Additionally, soil densification around the haunches and springlines of the culvert was performed using foot compaction in an attempt to ensure adequate soil support since the plate compactor could not reach those locations. The remaining burial depths were also achieved with a 200 mm soil lift, with the exception of 1.2 m, which required an additional 100 mm of backfill that was compacted to 90% standard Proctor using the same plate tamper. During the burial process the dry density and water content were recorded, and average values for each layer including the dry density as a percentage of the maximum achieved in a standard Proctor test are given in Table 1.

Instrumentation

Distributed strain measurements were obtained using nylon coated fiber optic sensors installed around the exterior of the culvert at a distance of 2.57 m from the West end of the specimen (directly below the actuator). This sensing fiber was adhered in a continuous loop to the centre of a crest and transitioned to the centre of an adjacent valley around the entire circumference using the approach described by Simpson et al. (2015). Fiber optic measurements were recorded using a Luna OBR 4600 fiber-optic strain analyzer (Luna, Roanoke, Virginia) before burial, upon the completion of each burial step and at each predetermined load step. The gauge length and sensor spacing for all scans were set at 20 mm for the entire experiment. Since fiber optic strain sensors are susceptible to temperature change, the culvert wall and ambient air temperatures were observed over the duration of the experiment. During each of the loading tests there was found to be less than 1 °C change in both temperatures, and thus the impact of temperature changes was considered negligible during individual load stages.

Additionally, six uniaxial foil strain gauges were also installed on the culvert exterior at certain positions on the circumference at a distance of 2.42 m from the West end. These gauges were attached in pairs, one centred on the crest and the other centred on the adjacent valley of the corrugation, at the crown, South springline and invert of the culvert. The strain gauges had a gauge length of 5 mm, resistance of 120 Ω ± 0.3%, gauge factor of 2.11 ± 1.0%, temperature compensation for steel thermal expansion of 11 PPM / °C and a thermal output of ± 2 $\mu\varepsilon$ / °C. The purpose of recording these discrete measurements was to check the validity of the fiber optic strain data through comparison. The fiber optic cables and strain gauges on the culvert are shown in Figure 2. Lastly, the vertical and horizontal diameters were monitored using string potentiometers installed 2.64 m from the West end.

Loading

At very shallow cover, single axle loading, as defined in the CHBDC, is most critical. Since the single axle features a centre to centre spacing of 1.8 m between the two wheel pairs (with a clear distance of 1.2 m between the patches of surface pressure) (CSA 2017b), these loads will not overlap for a culvert of the size and shallow cover depth being tested. Static vehicle loading was therefore simulated using loads from the actuator applied directly onto a single wheel pair configuration. The steel plate with dimensions of 0.25 m by 0.60 m was selected to represent the typical contact area of a wheel pair for a CL-625-ONT truck (CSA 2017b). Steel columns were also used to transfer the load from the actuator to the steel plate due to a significant height difference between the actuator and the ground surface (Figure 1(d)). All loading was applied pseudo-statically, and energy absorbed by the column and reaction frame had negligible influence on load transfer to the soil and pipe.

Since the culvert was to undergo additional testing after this experiment, the specimen could not be loaded to failure. Therefore, an upper load limit was selected as the lesser of either the largest factored service load or the load step at which peak strain in the culvert of 800 με [350 με below the yield strain (ASTM 2018)] was observed during the experiment. The test was halted at whichever limit occurred first. Factored service loads (P_f) were calculated based on both the Canadian [Equation ((3) (CSA 2017b)] and US [Equation ((4) (AASHTO 2017b)] standards where the single wheel pair load (P) of the design truck from each code was multiplied by the serviceability load factor and the dynamic load allowance. The serviceability load factor was taken as 0.9 and 1.0 from the Canadian and US codes, respectively. The dynamic load allowance, which varies with cover depth, was calculated according to clause 3.8.4.5.2 in the Canadian code [denoted as DLA (CSA 2017b)] and equation 3.6.2.2-1 in the US code [denoted as IM (AASHTO 2017b)]. In the US code the dynamic load allowance is a percentage.

$$P_f = P(1 + DLA)0.9 \tag{3}$$

$$P_f = P\left(1 + \frac{IM}{100}\right)1.0 \tag{4}$$

Consistent load steps were also selected based on the wheel pair load multiplied by the same serviceability factor, equalling 79 kN and 73 kN for the Canadian and US codes, respectively. Lastly, load steps of 25 kN and 50 kN were chosen since they represent approximately one third and two thirds of the largest consistent load values. Loading was halted to capture fiber optic data at each load increment, which are summarized in Table 2. However, during testing an additional load step of 35 kN was deemed necessary in the 0.1, 0.3 and 0.5 m tests based on the level of strain observed at the 25 kN load step. Finally, as stated earlier, the loading at each burial depth was applied in three cycles to observe the initial inelastic response and subsequent elastic unloading and reloading. It was observed that cycle 2 and 3 produced nearly identical strain results (as also reported by Regier et al. 2017), thus the remainder of this report will focus solely on responses during the first and third cycles.

Resultant Thrusts and Bending Moments

The strain values obtained from the fiber optic sensors were measured along the valley, $\mathcal{E}_1$, and the crest, $\mathcal{E}_2$, of the exterior of the culvert (its outer-most fiber). Since the cable installed in the valley does not represent the innermost fiber strain of the corrugation, $\mathcal{E}_{IF}$, the interior valley strain was approximated with linear extrapolation using Equation ((5) (Regier et al. 2017, 2018; Tetreault et al. 2018) also shown in Figure 3.

$$\mathcal{E}_{IF} = \left(\frac{\mathcal{E}_1 - \mathcal{E}_2}{h}\right) t + \mathcal{E}_1 \tag{5}$$

where: h = radial distance between gauges (mm) and t = intact wall thickness (mm). Then, the average strain, $\mathcal{E}_{ave}$, was calculated using this value and Equation ((6), which was then used to calculate the thrust per unit length, N (kN/m), with Equation ((7),

$$\mathcal{E}_{ave} = \frac{\mathcal{E}_2 + \mathcal{E}_{IF}}{2} \tag{6}$$

$$N = \mathcal{E}_{ave} EA \tag{7}$$

here E = the Young's modulus (MPa) and A = the wall cross-sectional area per unit length (mm^2/mm). In addition, the curvature per unit length, κ (10^{-6}/mm), and bending moment per unit length, M (kNm/m), were calculated using Equations ((8) and ((9), respectively. A positive curvature represents tensile strain on the outer surface and compressive strain on the inner surface of the culvert.

$$\kappa = \frac{\mathcal{E}_2 - \mathcal{E}_1}{h} \tag{8}$$

$$M = EI\,\kappa * 10^{-3} \tag{9}$$

Where I = the second moment of area per unit length of the wall cross-section (mm^4/mm). Finally, the yield thrust, and yield moment were calculated using Equations ((10) and ((11), respectively,

$$N_y = -\sigma_y A \quad (10)$$

$$M_y = -\sigma_y S \quad (11)$$

where σ_y = yield stress (230 MPa) and S = elastic section modulus per unit length (mm^3/mm).

Response from Pseudo-Static Surface Loading

All moment and thrust results discussed herein focus entirely on the response to live load and are incremental, meaning that the data is zeroed at the beginning of each respective cycle. No earth loading was considered here although earth load was considered in the section on diameter change. The response to earth loading, or weight of the soil mass above the culvert as well as the lateral restraint provided to the culvert by the soil under this weight, is recorded before live loading and subtracted from the data collected during each cycle. This facilitates direct comparisons between live load responses measured during the first and third load cycles. Furthermore, moment and thrust results have been plotted in polar coordinates rather than using an elliptical layout in order to avoid data overlapping in areas where the radius of the ellipse changes. Additionally, strain values at the South shoulder and North haunch were omitted in all analyses as these locations represent a circumferential joint and the transition of the fiber optic cable between crest and valley in the corrugation where the fiber was not bonded to the culvert.

Throughout the experiment, it was found that the two sensing technologies previously mentioned were in good agreement (within ±12 μƐ on average) at the invert and springline while the strain gauge values at the crown were 13% smaller on average than the fiber optic measurements. This was likely caused by the 0.15 m offset (two corrugation wavelengths) separating the strain gauges and the fiber optics (which were directly below the actuator), combined with the high variability of strain behaviour expected at the crown along the length of the culvert. Therefore, the strain gauge data will not be discussed further. In addition, the number of load steps achieved per cover depth was restricted by the predetermined 800 μƐ limit for depths less than 700 mm. This suggests that the minimum burial recommended in clause 12.6.6.3 of the

American code [300 mm (AASHTO 2017a)] permits some yield of the corrugated steel. Culverts with dimensions similar to those for the culvert used in this project may yield because the recorded strain approached the yield limit at a fraction of the total design service load. Alternatively, based on the cover depths used in this study, the Canadian minimum [600 mm (CSA 2017b)] appears to be near the point where the structure transitions from a high possibility of yield to elastic response under service loads. The peak load step and corresponding reason for limiting the load are given in Table 3.

Impact of Burial Depth

Since the 25 kN load step was the only load achieved at every depth during the experiment, a comparison was performed using the results at 25 kN at each level of cover to assess the impact of burial depth on the elliptical culvert. During cycle 1 at each depth, peak negative moments were observed at the crown directly below the simulated wheel pair and large positive moments occurred at each shoulder induced by the inward bending at the crown (see Figure 4(a)). Meanwhile, negligible strains around the bottom half of the culvert indicated that the bending moments were approximately zero in this area. At 100 mm of cover, the peak bending moment was observed to be -1.74 kNm/m, approximately 60% of the yield moment – calculated using Equation (11). When the depth increased to 300 mm (the minimum burial according to AASHTO (2017a)) the peak moment decreased to -0.78 kNm/m, i.e. 27% of the yield moment, and as the burial depth continued to increase towards 600 mm (the minimum burial according to CHBDC (2017b)) the peak moment became less than 10% of the yield moment. Once 600 mm burial depth was achieved, the peak moment continued to decrease, steadily approaching zero, but in increasingly smaller increments. Cycle 3 showed similar moment behaviour patterns with an 8% decrease in peak moment at 100 mm of cover and increased peak live load moments of 0.13 and 0.02 kNm/m for depths of 300 mm and 1200 mm, respectively (Figure 4(b)). When compared to the yield moment, at 100 mm the observed moment from cycle 3 decreased to 55% of yield while at 300 mm it increased to 30% of yield, in addition the other burial depths (500 to 1200 mm) also experienced similar increases. The decrease at 100 mm is because during cycle 1, the soil experiences both elastic and plastic deformation while in cycles 2 and 3 the soil experiences essentially only elastic deformation resulting in a reduced response in the culvert. Meanwhile, the increase at every other cover depth does not follow this trend and is believed to be caused in part by non-uniform soil modulus and inconsistent peak load values, which is discussed in more detail in the following section.

The thrust behaviour during cycle 1 displayed a peak negative value near the crown for each burial depth (Figure 5(a)). Thrust force then decreased towards the springlines and became zero between the haunches and across the invert indicating load shedding into the adjacent soil. A peak thrust value of -41 kN/m was seen at 100 mm which represents only 8% of the yield thrust – calculated using Equation (10) – while at 300 mm the recorded thrust became 6.5% of the yield limit. The thrust eventually fell below 3% of the yield limit once a cover of 600 mm was achieved. Cycle 3 showed very similar behaviour with changes in peak thrust as large as 5 kN/m which represents only a 1% difference relative to cycle 1 when compared to the yield thrust (Figure 5(b)). Based on the structural responses to the applied load of 25 kN that were measured at every burial depth, it appears that flexural behaviour remains higher than thrust behaviour at all cover depths. The moment rather than the thrust consistently represented a larger percentage of its respective yield limit (yield moment versus yield thrust).

It is understood that this interpretation of the most critical strength limit state (flexure rather than thrust) is conservative. It neglects the redundant nature of buried flexible pipe behaviour when subjected to bending since the load capacity is not fully mobilized when yield develops at an extreme fiber as a result of flexure. That is to say, even if a full plastic hinge develops at one location, the pipe will not likely collapse. This interpretation is considered prudent, however, since design against first yield under vehicle loads at the ground surface should avoid any potential for incremental collapse under repeated load cycles.

Impact of Live Load

The impact of the magnitude of the live load was assessed by comparing the culvert behaviour at 500 mm at each load step since at this depth, five of the seven predetermined load steps (from Table 2) were applied. It also represents a burial depth slightly below the 600 mm Canadian minimum cover depth (CSA 2017b). For this test, the maximum load applied was 79 kN, which was determined by the strain limit previously mentioned. This force is below the Canadian service load by 23% and the US service load by 15%.

During cycle 1 at each load step, the peak negative moment and thrust were again observed at or near the crown directly below the simulated wheel pair, while large positive moments developed at the shoulders (Figure 6(a) and Figure 7(a)). Similar to observations in the previous section, there were negligible moment and thrust around the bottom half of the culvert. At the largest load the peak moment in the culvert reached -1.49 kNm/m, which represented 51% of the steel's yield moment. In comparison, the peak thrust at the same applied load was -71 kN/m, only 13% of the yield thrust, suggesting again that bending moment is the more critical structural demand at this shallow burial depth.

The results observed during cycle 3 however, differ noticeably compared to cycle 1. At the first two load steps (25 and 35 kN) the recorded moment (Figure 6(b)) and thrust (Figure 7(b)) increase from cycle 1 to cycle 3. Then during the remaining load steps (50 – 79 kN) both moment and thrust decrease overall from cycle 1 to cycle 3 while also developing an upward (less negative) trend at the crown that becomes more apparent at larger applied loads. At each instance where a new larger peak load is achieved in cycle 1 there is a decrease in the response to that same load in cycle 3, in this analysis those loads are 50, 73 and 79 kN. This can be attributed to plastic deformation of the soil causing permanent strain during cycle 1 that does not transfer to cycle 3 because the data is zeroed at the start of each cycle. Furthermore, it is possible that patterns of soil modulus distribution are complicated by the compression of the backfill under overburden plus surface loading, which contributed to the increased response from cycle 1 to cycle 3 observed at loads of 25 and 35 kN in these experiments. This complication could be mitigated if the backfill was excavated and replaced for each burial depth, thus avoiding the effect of any previous surface loading. However, this was not possible logistically due to both cost and time constraints. Therefore, it is not possible at this time to provide detailed explanations of the changes in observed responses between cycle 1 and cycle 3 at lower applied loads. Despite this behaviour, bending moment remains more critical than thrust for cycle 3, with observed moment having a peak maximum value of -0.96 kNm/m and thrust reaching -56 kN/m, which represented 33% and 10% of their respective yield limits.

Extrapolated Culvert Behaviour

In typical culvert design, the structure must provide adequate resistance to the ultimate (strength) limit state. Furthermore, during construction and throughout its service life it is possible for a culvert in the field to encounter loading that causes strains greater than 800 με (close to or beyond yielding). The culvert in this project was not loaded to either the strength limit or the yield limit as it was to be used as part of a follow-on experimental campaign. Therefore, the results at each load step and cover depth were therefore extrapolated to the fully factored load, P_{FFL} (kN), which varies with depth, and then normalized using the yield thrust, N_y (kN/m) or yield moment, M_y (kNm/m), as per Equation (12) and (13), respectively below. This was done to assess the thrusts and moments at larger applied loads relative to the yield thrust and yield moment.

$$N_{ext} = \frac{N}{N_y} * \frac{P_{FFL}}{P_f} \tag{12}$$

$$M_{ext} = \frac{M}{M_y} * \frac{P_{FFL}}{P_f} \tag{13}$$

where N and M = the thrust (kN/m) and moment (kNm/m), respectively, at a given load step, P_f (kN). As the applied load increases towards the fully factored limit, the thrust and moment are expected to increase as well because stress is linearly related to strain for steel below the yield limit. If the structure's behaviour indicates the steel will yield before the fully factored load is reached, then the extrapolated value will be larger than 1. Meanwhile, a value of exactly 1 represents yield at the fully factored load and a value less than 1 suggests the culvert has more than sufficient capacity to resist the fully factored design loads. Although a culvert can continue to function after the steel has yielded, yield rather than the ultimate (fully plastic) thrust and moment capacities (i.e. collapse) will be examined in this assessment.

As mentioned previously, the predetermined strain limit restricted the number of load steps that were applied when testing at burial depths less than 700 mm. To compare the extrapolated data, an upper bound and a lower bound line were added to the plots discussed herein. The objective of these lines is to highlight an envelope of expected behaviour for this particular culvert since consistent load steps could not be tested at each burial depth. These boundaries also facilitate a clearer comparison between the peak response to initial loading and repeated loading (cycle 1 versus cycle 3) as well as thrust versus bending moment behaviour as a portion of the yield limit, which will be discussed later. It is important to reiterate that these results do not include the effect of earth loads, and that any value greater than 1 represents a linearly extrapolated moment or thrust demand that will likely have surpassed the yield loads of the culvert.

The extrapolated bending moment behaviour is shown in Figure 8 for both cycles 1 and 3. Under initial loading (cycle 1), the 25 kN line represents the lower bound moment, then as the applied force increases so too does the extrapolated moment. At depths less than 600 mm (Canadian minimum burial depth), the extrapolated moment at a single location is as much as five times greater than the yield limit indicating a projected demand that greatly exceeds yield resistance (the magnitude of moment that induces yielding). While this is a concern, it is also important to note that buried pipes are statically indeterminate structures and in order for a plastic collapse mechanism to occur, the pipe structure must yield in more than one location around the circumference (Regier et al. 2017). As cover increases, the upper bound moment is shown to decrease, eventually dropping below 1 once a 600 mm burial depth is achieved. Meanwhile, under repeated loading (cycle 3), despite a decrease in the extrapolated moment overall compared to cycle 1, the projected behaviour is still shown to be several times greater than the yield limit at depths less than 600 mm. Furthermore, in this cycle, the 25 kN line now represents the upper bound moment, and as the applied force increases, the projected (i.e. extrapolated) moment demand decreases.

The extrapolated thrust behaviour, as seen in Figure 9 for cycles 1 and 3, shows similar trends to the extrapolated moment behaviour. Under initial loading, the extrapolated thrust increases as the applied force increases, meanwhile the reverse is true under repeated loading (the third load cycle) which also has smaller thrust values than cycle 1. Additionally, as the burial depth increases, the extrapolated thrust decreases for both cycles. However, it is interesting to note that the thrust demand never exceeds the yield limit, suggesting that thrust does not govern the behaviour of this structure at shallow burial. In fact, Figure 10 (which compares the upper bounds of the extrapolated moment and thrust values for both first and third cycles) shows that at all burial depths and load cycles, the extrapolated moment is consistently larger than the extrapolated thrust. This data supports the findings of Regier et al. (2017) and Tetreault et al. (2018) who observed the formation of a plastic hinge when loading elliptical corrugated steel culverts to failure.

Diameter Change

Flexible culverts, such as the corrugated steel pipe tested in this experiment, tend to undergo horizontal and vertical diameter change during burial and as a result of live loads at the surface. While some deformation is expected, especially during burial when there is no benefit of soil restraint, excessive diameter changes can cause serviceability concerns. At shallow burial depths, diameter change becomes more of a concern because a larger percentage of the surface load reaches the culvert instead of dispersing through the soil and because the modulus, and therefore the stiffness, of the soil support is reduced at lower stress levels. The Canadian code recommends limiting diameter change during construction to 2% of the average nominal culvert diameter since anything larger can cause permanent deformations (CSA 2017b). However, this is based on mostly empirical considerations instead of analysis. In addition, the CHBDC and AASHTO do not provide any diameter change limits for metal pipes with dimensions similar to the one used in this experiment. However, a diameter change limit of 5% is often used in design and has been recommended as a result of the work by Spangler (1951).

Throughout the experiment, the vertical diameter of the culvert was monitored with a string potentiometer to determine the impact of surface loads at shallow burial on the serviceability limit states. The accumulated diameter change due to live load and earth load for cycles 1 and 3 are shown in Figure 11, where negative values represent an inward crown deflection. It is important to note that the 0 kN post-test readings do not match the 0 kN pre-test reading at the new, greater burial depth that follows. This is because it is common for flexible pipes to experience upward deformation at the crown during the early stages of burial – a phenomenon known as 'peaking' (CSA 2017a). A maximum accumulated vertical deflection of -6.36 mm was observed at a 79 kN applied force during the third cycle of the test at 1200 mm burial depth. This value is only 10% of the deflection limit (representing a 0.5% total diameter change) suggesting that serviceability limit states does not govern behaviour of this structure.

Conclusions

The objectives of this project were to undertake detailed load testing of one specific culvert at different burial depths to (1) investigate the change in behaviour as the burial depth transitions from shallow cover to deep cover, (2) investigate the impact of increasing static live loading on culverts with variable cover depths, (3) examine whether the vertical diameter change induced by combined earth and surface load meets the serviceability limit state at each depth, and (4) assess the implications and appropriateness of the current minima used for national highways in Canada and the US for this example culvert. An elliptical corrugated steel culvert was tested up to the factored service load limit or predetermined strain limit (to prevent yielding) at burial depths ranging from 100 mm to 1200 mm at regular intervals of 200 mm up to a depth of 900 mm followed by a final 300 mm interval. At each level of cover the load was increased by consistent load steps and was applied in three cycles to represent initial construction and/or highway loading (cycle 1) and repeated highway loading (cycle 3). The following conclusions were drawn from this investigation:

- Under a single wheel pair load positioned on the ground surface directly above the culvert crown, the maximum negative moment and thrust consistently occurred at the crown under shallow cover. Adjacent to the crown, large positive moments were also observed at the shoulders, suggesting inward bending near the top of the culvert. Meanwhile, load attenuation with depth to the adjacent soil and along the culvert was observed as negligible strains occurred across the bottom half of the culvert. This resulted in thrust and moment values that were approximately zero in this area.
- At depths up to and including 500 mm, the culvert reached the predetermined strain limit before the factored load limit could be achieved, indicating a high possibility that vehicle loads might yield

a corrugated steel culvert with similar dimensions and burial depth. This also suggests that the Canadian minimum burial depth (600 mm) is near the point where this particular soil-metal structure achieves enough capacity to resist the intended surface loads.

- To assess the impact of burial depth on the responses to initial loading and repeated loading, a 25 kN force was applied to the structure at each cover depth. During the first cycle and at 300 mm of cover (the AASHTO minimum) the recorded moment was at 27% of the yield moment while recorded thrust was only 6.5% of the yield thrust. When the burial depth was increased to 700 mm (above the 600 mm minimum Canadian requirement) the moment fell below 10% and the thrust decreased to less than 3% of the respective yield limits. Similar differences between moment and thrust were also observed during the third cycle of testing. This suggests that the bending moments (flexural behaviour) are more dominant than thrusts for this shallow buried culvert.
- To assess the culvert response under initial application of the live load, and then under repeated loading, the culvert behaviour was compared over 5 different load increments at a depth of 500 mm. During both cycles 1 and 3, the bending moment was consistently the dominant loading carrying mechanism when compared to thrust, achieving peak maximum values equal to 51% and 33% of the yield moment versus observed thrusts that reached 13% and 10% of the yield thrust.
- All calculated thrust and moment values were also extrapolated using the yield limit stress and fully factored limit loads to allow for assessment of the culvert at greater vehicle loads than were achieved during testing (extrapolation to fully factored loads). This revealed that bending moment consistently represented a larger percentage of the allowable capacity than thrust, indicating again that moment is more of a concern for this elliptical corrugated steel culvert at shallow burial. For instance, at cover depths less than the minimum level, the extrapolated incremental moment was as much as 5 times greater than the yield limit of the corrugated steel plate, while the thrust remained below 60% of the yield limit under the same conditions.
- Serviceability with regards to deformation was monitored during initial loading and repeated loading using string potentiometers. During the experiment the culvert only experienced a peak vertical diameter change of 0.5%, well below the 2% (CSA 2017b) and 5% (Spangler 1951) recommended

limits. Even when deflection was extrapolated to the values estimated at fully factored service loads, the values consistently remained below the limit, achieving extrapolated deformation values around 1% at the largest applied load, suggesting that deformation is not a short term concern for the particular culvert and backfill choices used for this study.

Data Availability Statement

All data generated or used during the study are available from the corresponding author by request.

Acknowledgements

The authors would like to thank the Canadian Foundation for Innovation and the Ontario Ministry of Research and Innovation for their generous financial support of the testing facilities used during this project. The tests and the post-test analyses were funded by the Natural Sciences and Engineering Research Council of Canada. The authors also thank Graeme Boyd, Josh Coghlan, and Rob Cichocki for their assistance.

References

AASHTO. (2017a). “Section 12: Buried Structures and Tunnel Liners.” *AASHTO LFRD Bridge Design Specifications*, LRFD, American Association of State Highway and Transportation Officials (AASHTO), Washington, DC.

AASHTO. (2017b). “Section 3: Loads and Load Factors.” *AASHTO LFRD Bridge Design Specifications*, LRFD, American Association of State Highway and Transportation Officials (AASHTO), Washington, DC.

ASTM. (2017). *Standard Practice for Classification of Soils for Engineering Purposes*. *D2487-17*, 10.

ASTM. (2018). *Standard Specification for Steel Sheet, Metallic-Coated by the Hot-Dip Process for Corrugated Steel Pipe*. *A929/A929M*, 5.

CSA. (2017a). “Section C7 Buried Structures.” *Commentary on CSA S6-14, Canadian Highway Bridge Design Code*, CSA, CSA Group, Mississauga, Ontario, Canada, 349–383.

CSA. (2017b). *Canadian Highway Bridge Design Code*. CSA, Canadian Standards Association (CSA) Group, Mississauga, Ontario, Canada.

CSPI. (2010). *Handbook of Steel Drainage & Highway Construction Projects*. Corrugated Steel Pipe Institute, Cambridge, Ontario, Canada.

Duncan, J. M. (1978). "Soil-Culvert Interaction Method for Design of Metal Culverts." *Transportation Research Board*, (678), 53–59.

El-Sawy, K. M. (2003). "Three-dimensional modeling of soil-steel culverts under the effect of truckloads." *Thin-walled Structures*, 41(8), 747–768.

Mai, V. T., Hoult, N., and Moore, I., D. (2014). "Effect of Deterioration on the Performance of Corrugated Steel Culverts." *Journal of Geotechnical and Geoenvironmental Engineering*, 140(2), 1–11.

Moore, I., D. (2012). "Large-scale laboratory experiments to advance the design and performance of buried pipe infrastructure." *Proc., 3rd Int. Conf. on Pipelines and Trenchless Technology*, ASCE, Reston, VA, 805–815.

Moore, I., D., and Brachman, R. W. (1994). "Three-dimensional analysis of flexible circular culverts." *Journal of Geotechnical Engineering*, 120(10), 1829–1844.

Regier, C., Hoult, N., and Moore, I., D. (2017). "Laboratory Study on the Behaviour of a Horizontal-Ellipse Culvert during Service and Ultimate Load Testing." *Journal of Bridge Engineering*, 22(3).

Regier, C., Moore, I., D., and Hoult, N. (2018). "Laboratory Study of the Remaining Strength of Deteriorated Corrugated Steel Culverts." *Journal of Pipeline Systems Engineering and Practice*, 9(2).

Sargand, S. M., White, K., Masada, T., and Wang, C. (2018). "Evaluation of Load-Rating Procedure for Metal Culverts under Shallow Soil Covers." *Journal of Pipeline Systems Engineering and Practice*, 9(1).

Seed, R. B., and Raines, J. R. (1988). "Failure of Flexible Long-Span Culverts Under Exceptional Live Loads." *Transportation Research Board*, (1191), 22–29.

Sezen, H., Yeau, K. Y., and Fox, P. J. (2008). "In-Situ Load Testing of Corrugated Steel Pipe-Arch Culverts." *Journal of Performance of Constructed Facilities*, 22(4), 245–252.

Simpson, B., Hoult, N., and Moore, I. (2015). “Distributed Sensing of Circumferential Strain Using Fiber Optic during Full-Scale Buried Pipe Experiments.” *Journal of Pipeline Systems Engineering and Practice*, 6(4).

Spangler, M. G. (1951). “Underground Conduits.” *Soil Engineering*, International Textbooks in Civil Engineering, International Textbook Company, Scranton, Pennsylvania, 409–449.

Taleb, B., and Moore, I., D. (1999). “Metal Culvert Response to Live Loading: Perfromance of Three-Dimensional Analysis.” *Transportation Research Board*, 1656(1), 37–44.

Tetreault, J., Hoult, N., and Moore, I. (2018). “Pre- and post-rehabilitation behaviour of a deteriorated horizontal ellipse culvert.” *Canadian Geotechnical Journal*, 55(3), 329–342.

Yeau, K. Y., and Sezen, H. (2012). “Load-Rating Procedures and Performance Evaluation of Metal Culverts.” *Journal of Bridge Engineering*, 17(1), 71–80.

Yeau, K. Y., Sezen, H., and Fox, P. J. (2009). “Load Performance of In Situ Corrugated Steel Highway Culverts.” *Journal of Performance of Constructed Facilities*, 23(1), 32–39.

List of Tables

Table 1: Summary of Backfill Properties

Soil Location	**Dry Density** $\left(\frac{g}{cm^2}\right)$	**Water Content (%)**	**Standard Proctor (%)**
Bedding	2.05	2.4	89.8
Invert – Crown	2.06	2.9	90.2
0 – 600 mm Cover	2.07	3.3	90.9
600 – 1200 mm Cover	2.13	4.0	93.5

Table 2: Applied Load Increments for Corrugated Steel Culvert Tests at Each Burial Depth (Peak Loads Shown in Table 3)

Load Step	**Load (kN)**
Initial Conditions	0
1	25
2	35
3	50
4	73
5	79
6	AASHTO Full Service
7	CHBDC Full Service
Post Test	0

Table 3: Peak Load Step and Loading Limit Achieved at Each Burial Depth for Shallow Cover Tests

Burial Depth (mm)	**Peak Load Step (kN)**	**Limit**
100	35	Strain (800 μƐ)
300	50	Strain (800 μƐ)
500	79	Strain (800 μƐ)
700	99	CHBDC Full Service Load
900	96	CHBDC Full Service Load
1200	91	CHBDC Full Service Load

List of Figures

A) B)

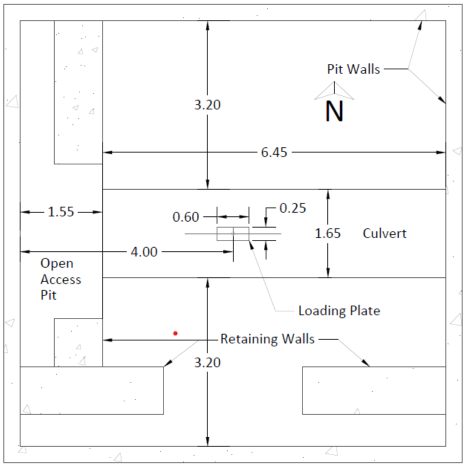

C) D)

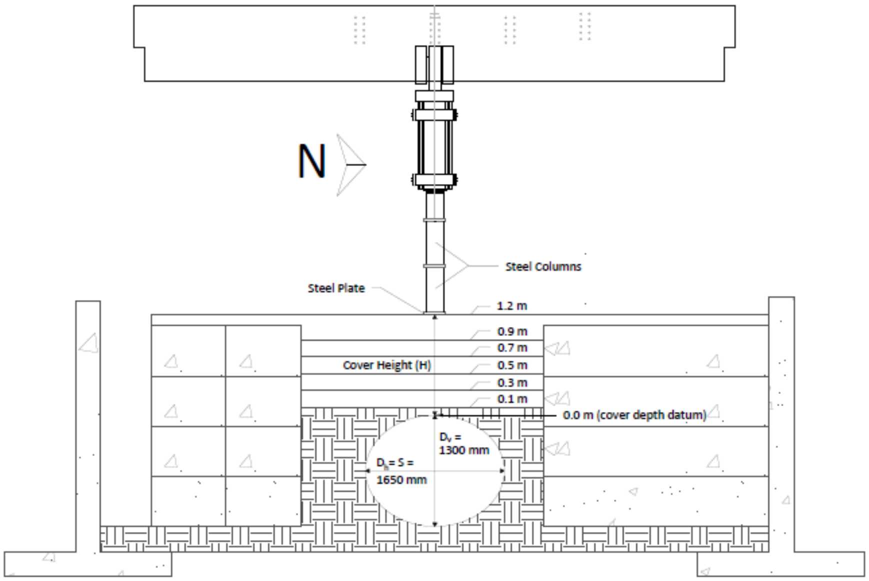

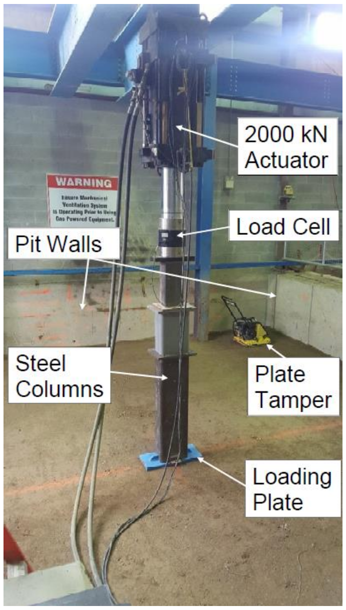

Figure 1: Corrugated steel culvert (a) the specimen before burial, (b) top view of test set up, (c) front view of test set up, and (d) load application configuration

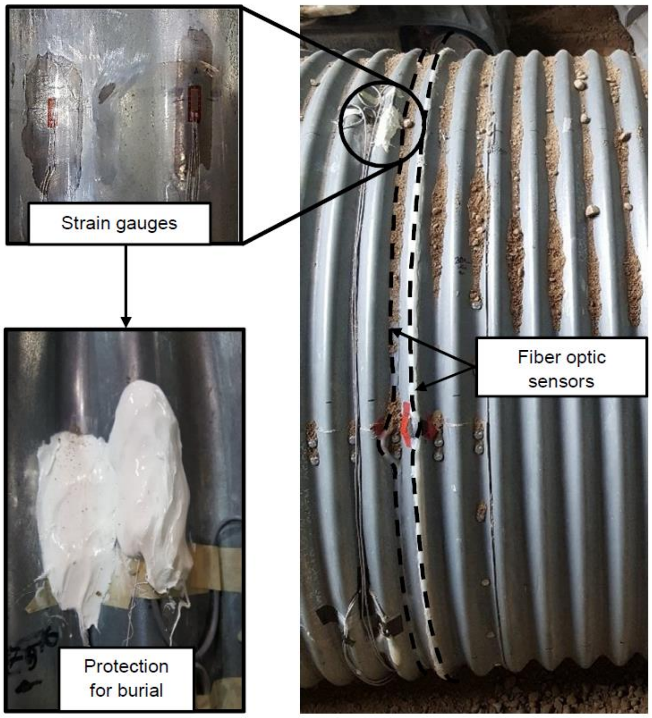

Figure 2: Fiber optic sensor (highlighted with black lines) and strain gauge (indicated with circles) locations

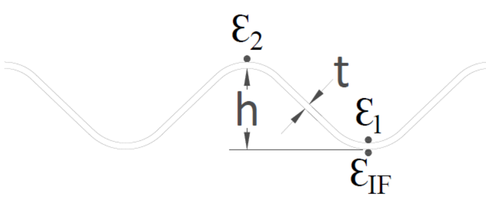

Figure 3: Fiber optic cable layout for linear extrapolation calculation

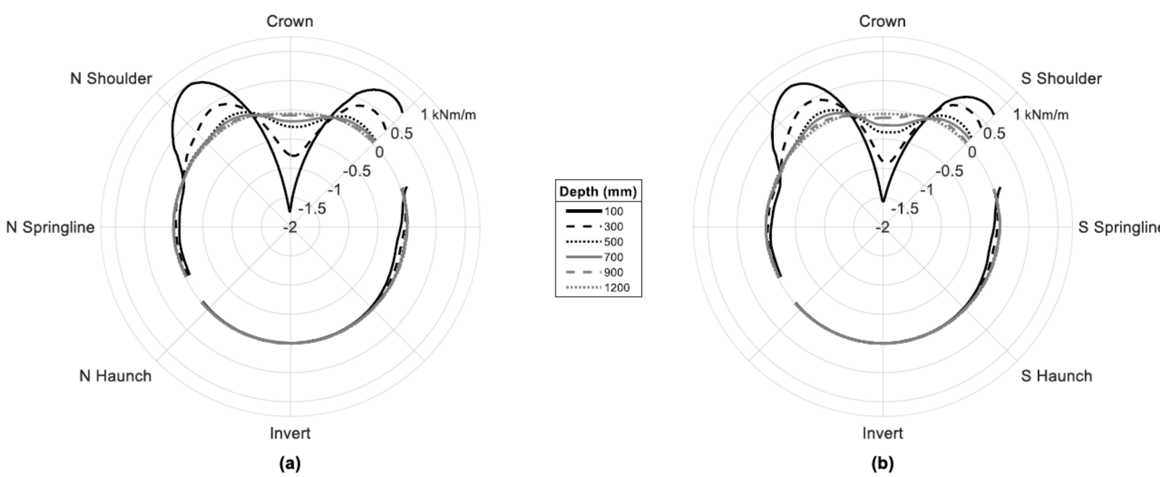

Figure 4: Moment distributions (kNm/m) for different cover depths at 25 kN for initial loading, (a) cycle 1, and repeated loading, (b) cycle 3

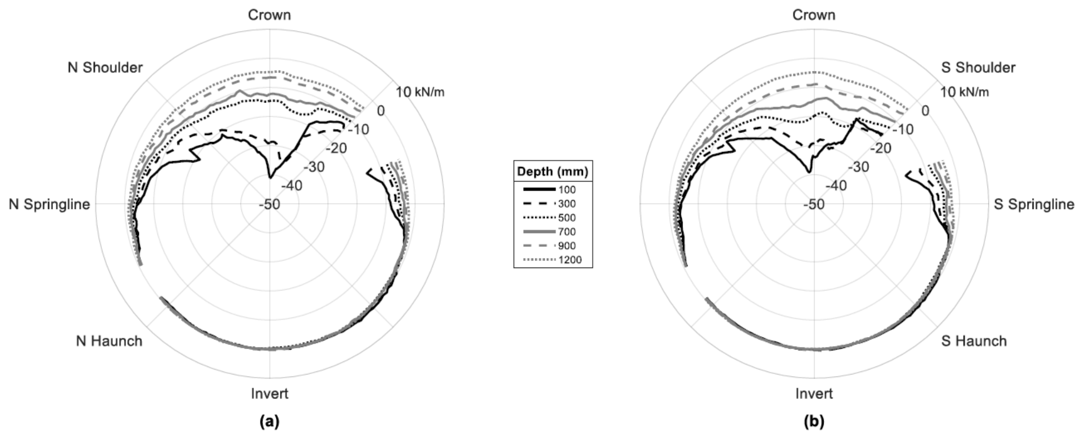

Figure 5: Thrust distributions (kN/m) for different cover depths at 25 kN for initial loading, (a) cycle 1, and repeated loading, (b) cycle 3

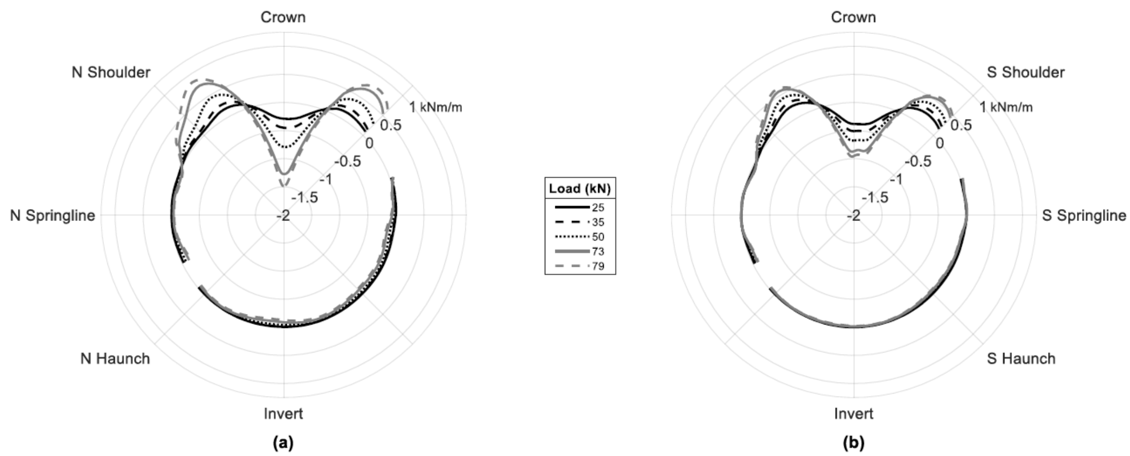

Figure 6: Moment (kNm/m) at 500 mm of cover for initial loading, (a) cycle 1, and repeated loading, (b) cycle 3

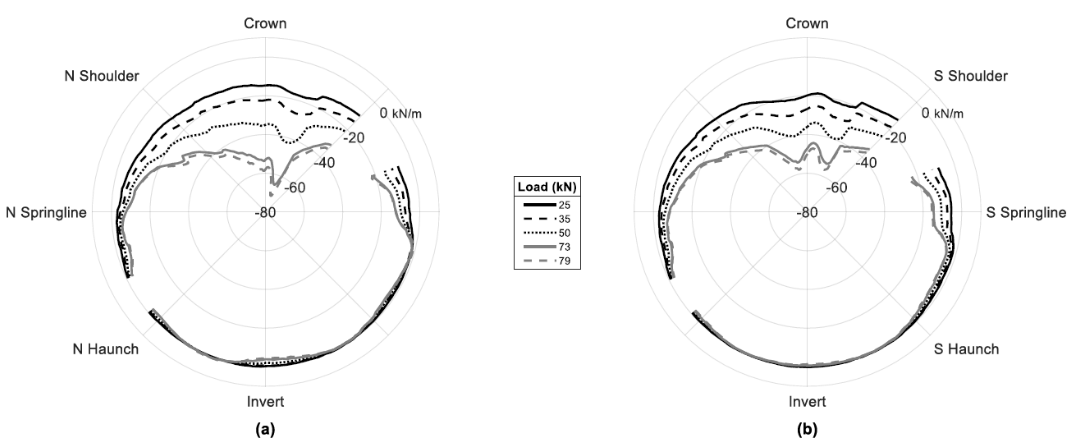

Figure 7: Thrust (kN/m) at 500 mm of cover for initial loading, (a) cycle 1, and repeated loading, (b) cycle 3

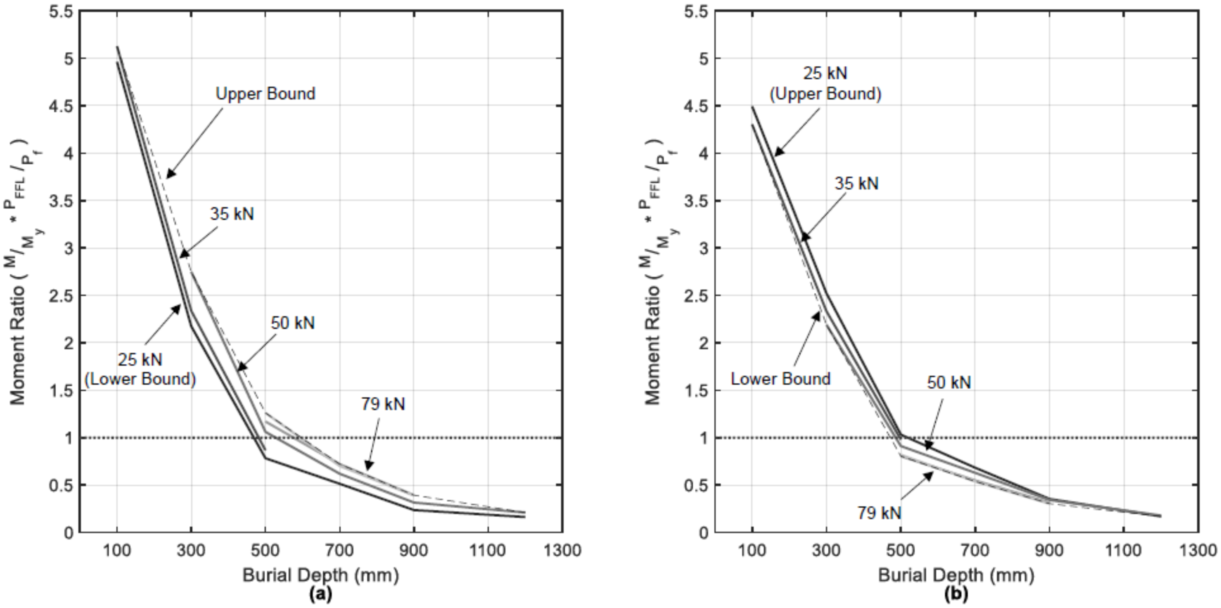

Figure 8: Moment extrapolated to the fully factored wheel pair load (a) cycle 1 and (b) cycle 3

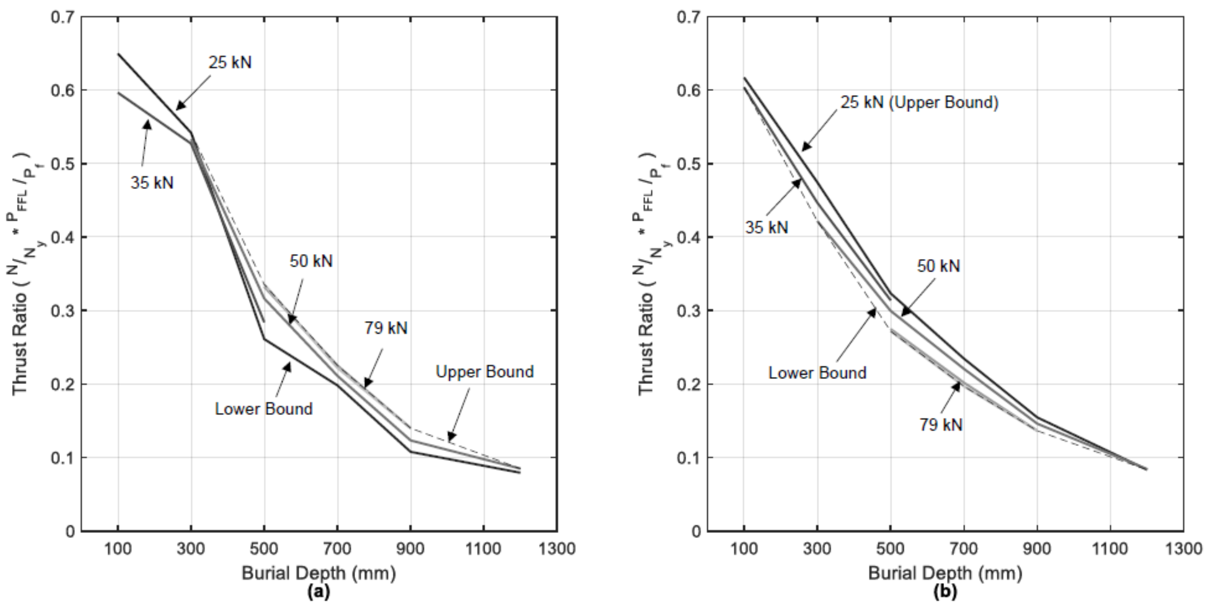

Figure 9: Thrust extrapolated to the fully factored wheel pair load (a) cycle 1 and (b) cycle 3

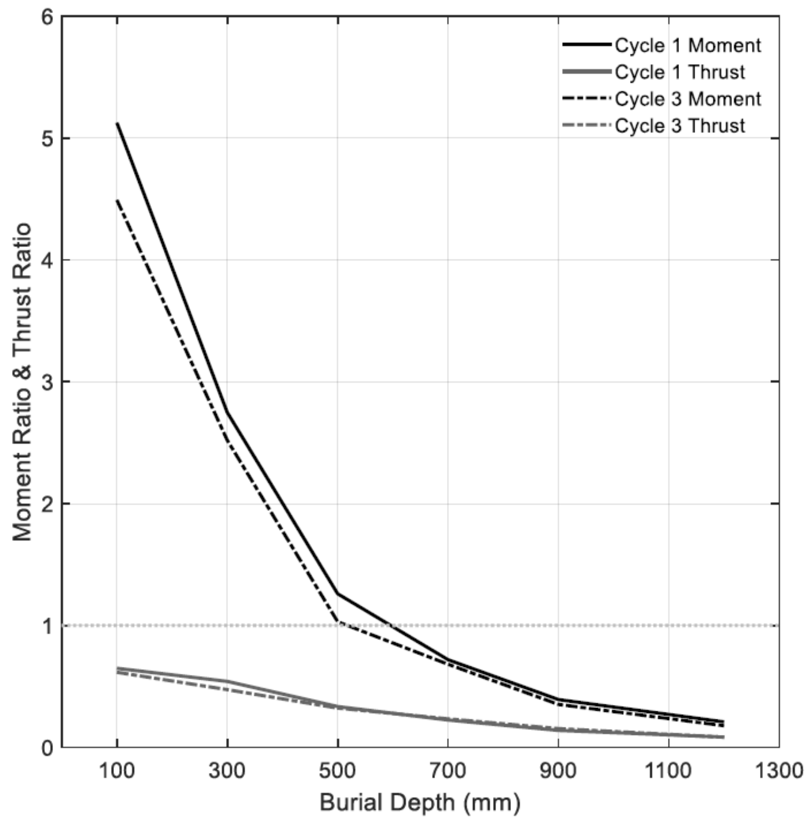

Figure 10: Upper bound comparison of extrapolated moment and thrust of cycle 1 and cycle 3

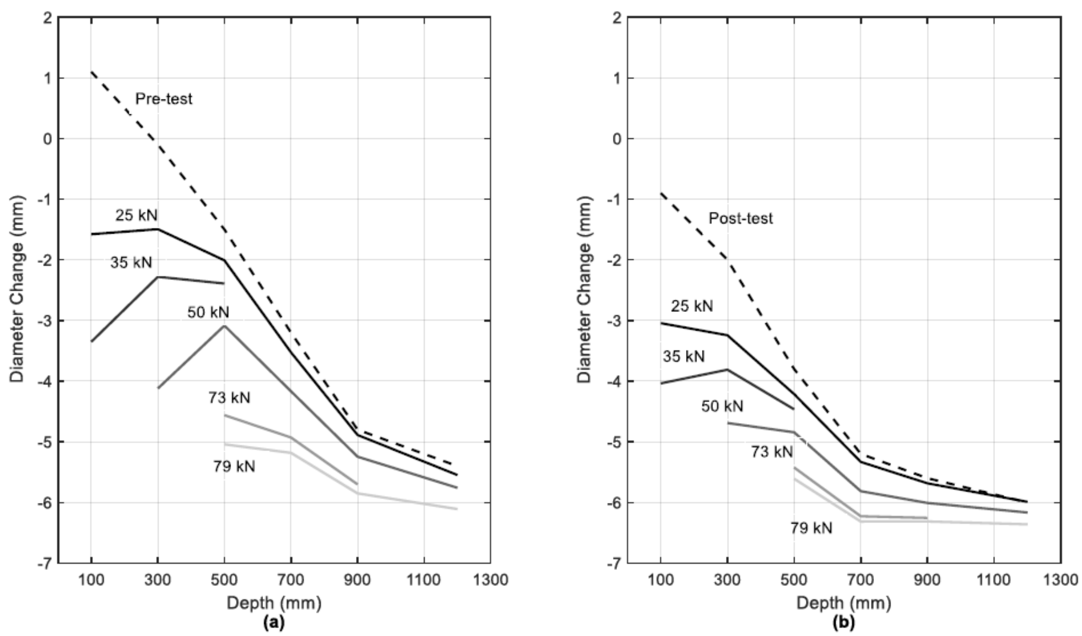

Figure 11: Accumulated vertical diameter change (a) cycle 1 and (b) cycle 3